

Extraction of inhomogeneous broadening and nonradiative losses in InAs quantum-dot lasers

Weng W. Chow¹, Alan Y. Liu, Arthur C. Gossard, and John E. Bowers

Citation: *Appl. Phys. Lett.* **107**, 171106 (2015); doi: 10.1063/1.4934838

View online: <http://dx.doi.org/10.1063/1.4934838>

View Table of Contents: <http://aip.scitation.org/toc/apl/107/17>

Published by the [American Institute of Physics](#)

Articles you may be interested in

[Sub-wavelength InAs quantum dot micro-disk lasers epitaxially grown on exact Si \(001\) substrates](#)

Applied Physics Letters **108**, 221101 (2016); 10.1063/1.4952600

AIP | Applied Physics
Letters

Save your money for your research.
It's now **FREE** to publish with us -
no page, color or publication charges apply.

If your article has the
potential to shape the future of
applied physics, it BELONGS in
Applied Physics Letters

Extraction of inhomogeneous broadening and nonradiative losses in InAs quantum-dot lasers

Weng W. Chow,^{1,a)} Alan Y. Liu,² Arthur C. Gossard,^{2,3} and John E. Bowers^{2,3}

¹Sandia National Laboratories, Albuquerque, New Mexico 87185-1086, USA

²Materials Department, University of California Santa Barbara, Santa Barbara, California 93106, USA

³Department of Electrical and Computer Engineering, University of California Santa Barbara, Santa Barbara, California 93106, USA

(Received 2 May 2015; accepted 18 October 2015; published online 28 October 2015)

We present a method to quantify inhomogeneous broadening and nonradiative losses in quantum dot lasers by comparing the gain and spontaneous emission results of a microscopic laser theory with measurements made on 1.3 μm InAs quantum-dot lasers. Calculated spontaneous-emission spectra are first matched to those measured experimentally to determine the inhomogeneous broadening in the experimental samples. This is possible because treatment of carrier scattering at the level of quantum kinetic equations provides the homogeneously broadened spectra without use of free parameters, such as the dephasing rate. We then extract the nonradiative recombination current associated with the quantum-dot active region from a comparison of measured and calculated gain versus current relations. © 2015 AIP Publishing LLC. [<http://dx.doi.org/10.1063/1.4934838>]

InAs based quantum-dot (QD) lasers emitting in the 1.3 μm wavelength regime are extensively investigated because of important applications involving data centers and optical communication. To optimize material and device design, it is important to have accurate details on gain and recombination processes, for example, quantitatively precise information regarding inhomogeneity and loss contributions in the fabricated samples. In this letter, we demonstrate an approach based on comparison of the results of a microscopic laser theory with threshold gain versus threshold current dependence obtained from experiment to quantify the degree of inhomogeneous broadening as well as the non-radiative loss rate for InAs dots-in-a-well (DWELL) lasers emitting at 1.3 μm . This method is also applied to the familiar InGaAs/GaAs quantum-well (QW) laser system emitting at 980 nm as a reference standard and for comparison with the QD lasers. Application of the approach to QW lasers may be found in the literature.¹

To begin, the calculated and measured spontaneous emission spectra are compared to extract the inhomogeneous broadening in as-grown samples. Then, the measured threshold modal gain versus threshold current density curves are fitted using the extracted inhomogeneous broadening value to estimate the carrier loss rate due to nonradiative recombination. The approach requires precise knowledge of the homogeneously broadened (intrinsic) gain and spontaneous emission spectra, without the use of free parameters. This is accomplished by treating dephasing effects from carrier-carrier and carrier-phonon scattering at the level of quantum kinetic equations.² The significantly more rigorous treatment distinguishes this approach from the more widely used ones, where scattering effects are described phenomenologically by introducing a free parameter, the dephasing rate.³ Calculated results for QWs compare very well with the experiment as shown previously⁴ and is again verified here. The extension to QDs is more complicated, requiring, for example, a non-perturbative

treatment of carrier-longitudinal-optical (LO) phonon scattering based on the polaron picture.^{5,6} This letter presents a first theory/experiment comparison of the approach for QD lasers.

The theoretical part of our approach is based on a first-principles calculation of the material gain G_{material} . The concept of material gain is introduced to allow investigation or evaluation of active medium performance independent of the optical resonator of the laser. From semiclassical laser theory,⁷ the material gain is given by

$$G_{\text{material}}(\omega) = -\frac{\omega}{\epsilon_0 n c V E(\omega)} \text{Im} \left(\sum_{\alpha, \beta} \mu_{\alpha\beta} p_{\alpha\beta} \right), \quad (1)$$

where ϵ_0 and c are the permittivity and speed of light in vacuum, $\mu_{\alpha\beta}$ is the dipole matrix element, n is the background refractive index, $E(\omega)$ is the laser electric field amplitude, ω is its frequency, V is the QW volume, and the summation is over all QD and QW states α and β , connected by dipole matrix element $\mu_{\alpha\beta}$. The polarization from electron-hole pairs in the QDs and QW $p_{\alpha\beta}$ is obtained from the steady-state solution to following equation:

$$\frac{dp_{\alpha\beta}}{dt} = i\omega_{\alpha\beta} p_{\alpha\beta} - i\Omega_{\alpha\beta} \left(n_{\alpha}^e + n_{\beta}^h - 1 \right) + S_{\alpha\beta}^{c-p} + S_{\alpha\beta}^{c-c}, \quad (2)$$

which belongs to the semiconductor Bloch equations.⁸ In Eq. (2), $\omega_{\alpha\beta}$ and $\Omega_{\alpha\beta}$ are the renormalized transition and Rabi frequencies, n_{α}^e and n_{β}^h are the electron and hole populations, which are obtained assuming Fermi-Dirac distributions for a total carrier density N . The complex correlations, $S_{\alpha\beta}^{c-p}$ and $S_{\alpha\beta}^{c-c}$, account for dephasing from carrier-phonon and carrier-carrier scattering, respectively. The details for their evaluation are described in the literature.²

The spontaneous emission spectrum may be obtained from the material gain spectrum by detailed balance⁹

$$S(\omega) = \frac{1}{\hbar} \left(\frac{n\omega}{\pi c} \right)^2 G_{\text{material}}(\omega) \left[e^{(\hbar\omega - \mu_{eh})/(k_B T)} - 1 \right]^{-1}, \quad (3)$$

^{a)}Electronic mail: wwchow@sandia.gov

where k_B is the Boltzmann constant, T is the temperature, and μ_{eh} is the electron-hole chemical potential energy separation, which is the energy at crossover from gain to absorption in the gain spectrum. Finally, to account for the effects of inhomogeneous broadening due to sample dimensional or alloy fluctuations, we performed a statistical average over a range of band-gap energy ε

$$\mathcal{F}_{inh}(\omega) = \int_{-\infty}^{\infty} d\varepsilon \frac{1}{\sqrt{2\pi}\Delta_{inh}} e^{-(\varepsilon-\varepsilon_g)^2/(\sqrt{2}\Delta_{inh})^2} \mathcal{F}(\omega, \varepsilon), \quad (4)$$

where ε_g is the InAs band-gap energy, and we assume a weighting described by a normal distribution characterized by an inhomogeneous broadening width Δ_{inh} . $\mathcal{F}(\omega, \varepsilon)$ is the homogeneous gain or spontaneous emission spectrum, $G_{material}(\omega)$ or $S(\omega)$, respectively, where we added the parameter ε to indicate that the homogeneously broadened quantities are computed for a precise electronic structure.

The input for the calculations are the electronic structure properties, specifically the electron and the hole energy levels, as well as the optical dipole matrix elements. They are computed using a Schrödinger/Poisson solver,¹⁰ where the input is the heterostructure and bulk material parameters. For the laser devices used in the experiment, the QD active region consists of five 8 nm $\text{In}_{0.15}\text{Ga}_{0.85}\text{As}$ QWs separated by 37.5 nm GaAs barriers, where each QW embeds InAs QDs (DWELL structure). Similar QW lasers where the active region consists of three 8 nm $\text{In}_{0.2}\text{Ga}_{0.8}\text{As}$ QWs were also measured for comparison. In both cases (QD and QW), the entire active region is cladded by 30 nm $\text{Al}_{0.2}\text{Ga}_{0.8}\text{As}$ layers, which in turn is sandwiched between 1.5 μm thick $\text{Al}_{0.4}\text{Ga}_{0.6}\text{As}$ layers (see Figure 1). The structures used in the photoluminescence measurements consisted of a single DWELL cladded on either side by GaAs (50 nm)/ $\text{Al}_{0.4}\text{Ga}_{0.6}\text{As}$ (50 nm). The material gain $G_{material}(\omega)$ is calculated for a sheet of InAs QDs embedded in an 8 nm $\text{In}_{0.15}\text{Ga}_{0.85}\text{As}$ QW layer with QD density N_{dot} .

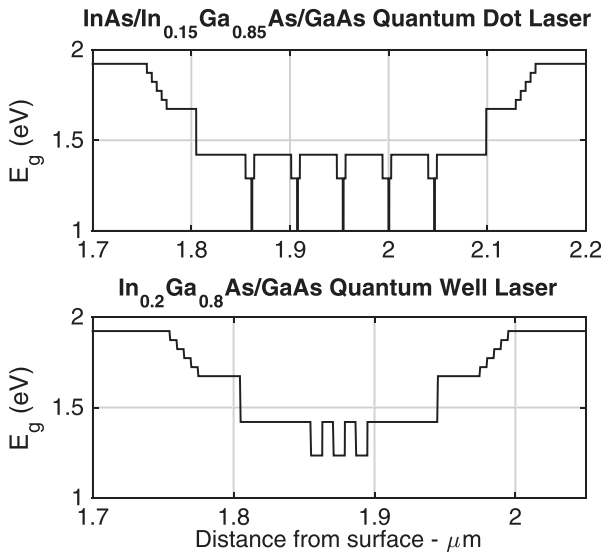


FIG. 1. Band diagrams for both the $\text{InAs}/\text{In}_{0.15}\text{Ga}_{0.85}\text{As}$ QD laser (top) and the $\text{In}_{0.2}\text{Ga}_{0.8}\text{As}$ QW laser (bottom). Both types of active regions are embedded in a $\text{GaAs}/\text{Al}_{0.2}\text{Ga}_{0.8}\text{As}$ separate confinement heterostructure which is step graded to the $\text{Al}_{0.4}\text{Ga}_{0.6}\text{As}$ cladding layers.

Modal gain versus current density was determined from pulsed (0.5% duty cycle) light versus current (L-I) measurements on broad-area laser stripes 50 μm wide and various cleaved cavity lengths. A total of 108 and 126 different QD and QW lasers were measured, respectively. The reciprocal differential slope efficiency per cavity length was plotted versus cavity length, from which the waveguide optical loss (α_{abs}) and injection efficiency (η) were extracted using a linear fit.¹¹ Following convention, the injection efficiency refers to the fraction of injected current entering the active region.¹¹ The threshold modal gain is determined by the round-trip gain equal loss condition

$$G_{modal}^{th} = \frac{1}{2L} [\alpha_{abs} - \ln(R_1 R_2)]. \quad (5)$$

Here, we assume reflectivities of $R_1 = R_2 = 0.32$ for the uncoated as-cleaved facets, as well as negligible losses in the mirrors (i.e., all light not reflected back into the mode by the mirror was externally transmitted outside the cavity). The extracted values of for the average injection efficiency and their uncertainties from this analysis are $\eta = 0.61 \pm 0.04$, $\alpha_{abs} = 3.17 \pm 0.41 \text{ cm}^{-1}$ for the QD lasers; and $\eta = 0.64 \pm 0.03$, $\alpha_{abs} = 6.79 \pm 0.59 \text{ cm}^{-1}$ for the QW lasers.

There is concern of a systematic error in applying this traditional method of analysis for quantum dot lasers, as this method assumes that the carrier density (and η) is pinned at threshold, which may not always be the case in quantum dot lasers as was discussed in Ref. 12. More measurements and simulations, beyond the scope of the present investigation, will be necessary to address this issue, e.g., more precise fitting of the spontaneous emission spectrum using arbitrary carrier distributions. A sensitivity analysis will be presented to quantify the uncertainty that this systematic error may induce in our conclusion.

Figure 2(a) shows the homogeneously broadened TE (transverse electric) material gain spectra computed for room temperature and a range of carrier densities. The TM (transverse magnetic) gain is highly attenuated because of compressive strain. The lowest density spectrum indicates only ground-state gain. At higher energies are the excited-state absorption resonances. The QD resonances exhibit carrier-density dependent energy shifts and broadening that are observed in experiments^{13,14} and discussed in detail elsewhere.¹⁵ These intrinsic features are typically not observed in the present samples because of the smoothing process of inhomogeneous broadening. To illustrate the effects of inhomogeneous broadening, Eq. (4) is used to convert the homogeneously broadened gain spectra to inhomogeneously broadened ones. Figure 2(b) plots the result for a carrier density of $N = 4 \times 10^{11} \text{ cm}^{-2}$. With increasing inhomogeneous broadening, the gain spectrum began to resemble that observed in the present experiment.¹⁶ For this study, the most important effect of inhomogeneous broadening is degradation in peak gain.

To obtain a quantitative estimation of inhomogeneous broadening, we looked at the spontaneous-emission spectrum. A 785 nm laser with approximately 26 W/cm^2 incident power density was used. This is sufficient to saturate the ground-state QD luminescence and significantly populate the

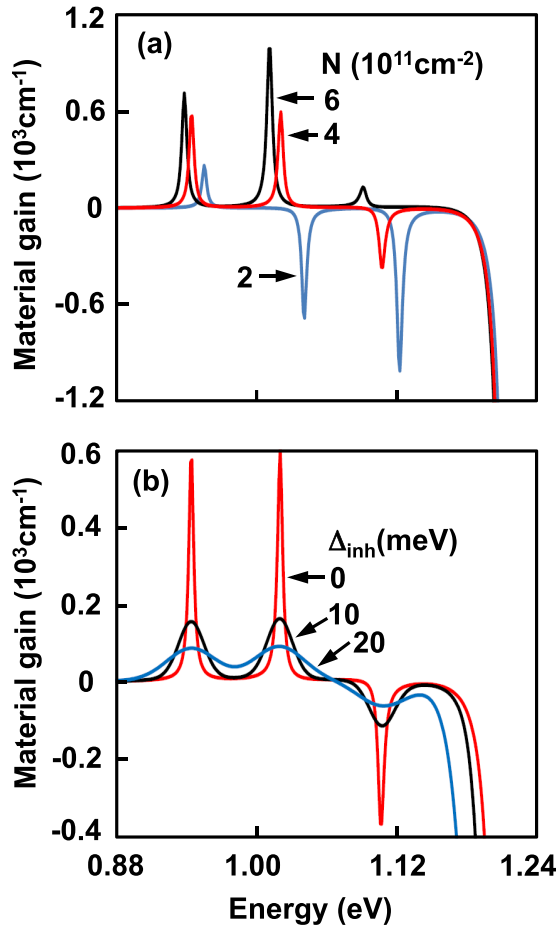


FIG. 2. (a) Homogeneously broadened ($\Delta_{inh}=0$) gain spectra for carrier densities as indicated. (b) Gain spectra for carrier density $N=4 \times 10^{11} \text{cm}^{-2}$ and inhomogeneous broadening as indicated.

higher excited states. The dotted curve in each panel of Fig. 3(a) shows the experimental spontaneous-emission spectrum, measured with a normal-incidence room-temperature photoluminescence setup for a single sheet of InAs QDs. The y-axis scaling is from the theory. We did not calibrate the measurement apparatus. In fact, as in the case for QWs, the theory/experiment fitting may be used to calibrate the experiment. The experimental spontaneous-emission spectrum is

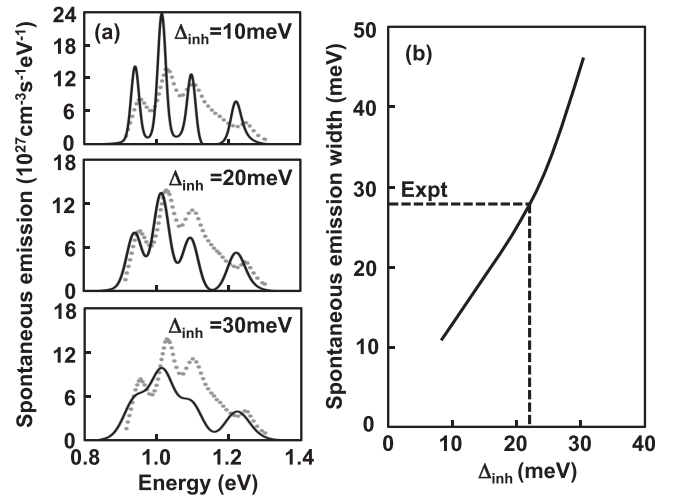


FIG. 3. (a) Measured (dotted curve) and calculated (solid curve) spontaneous-emission spectra. The y-axis scaling is from the theory, and the amplitude in the experimental spectra is adjusted to match the theory. The calculated spectra are for carrier density $N=5 \times 10^{11} \text{cm}^{-2}$ and inhomogeneous broadenings as indicated. (b) Calculated spontaneous-emission linewidth versus inhomogeneous broadening. The dashed line indicates the spontaneous-emission linewidth determined from experiment and the corresponding inhomogeneous broadening according to fit to theory.

fitted to the sum of three Lorentzian functions, where the peak positions and amplitudes were adjusted together with a common linewidth. We did not attempt to fit the overall shape partly because we did not include all the InAs QD bound-state transitions in the gain calculation. However, the entire bound-state transitions and the continuum are used to determine the chemical potential.

A spontaneous emission linewidth of 28 meV (which included both homogeneous and inhomogeneous contributions) gave the best fit of the experimental spectrum. To extract the inhomogeneous-broadening linewidth Δ_{inh} , we used Eqs. (3) and (4) to compute the spontaneous-emission spectra for a range of Δ_{inh} 's (solid curves in Fig. 3(a)). The same fitting to the sum of three Lorentzian functions is performed and the result is plotted in Fig. 3(b). According to the dashed lines, the measured spontaneous-emission linewidth of 28 meV translates to an inhomogeneous broadening of $\Delta_{inh} = 22 \text{meV}$. Considering the approximate level of the

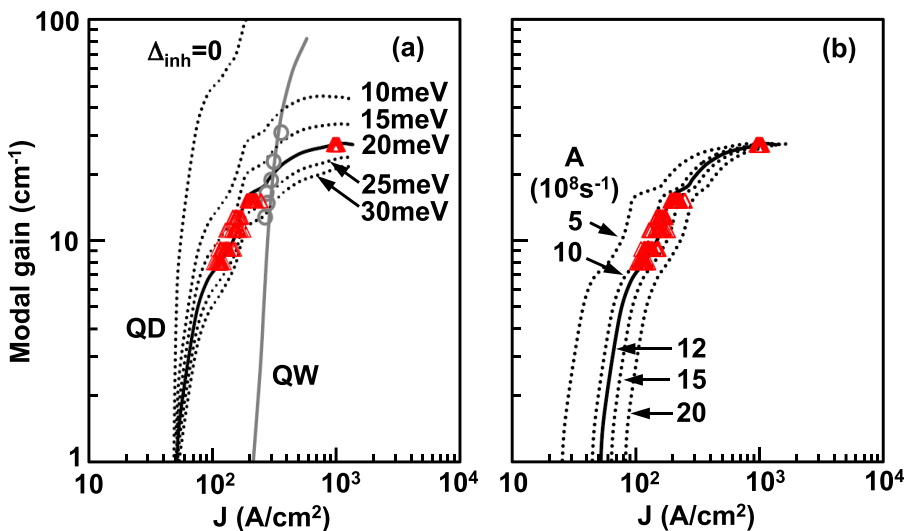


FIG. 4. (a) Calculated QD modal gain versus current density curves for inhomogeneous broadening as labeled. The calculated curve for QW is the grey curve. The data points are from measurements: QD (triangles) and QW (circles). The curves are computed for $A=1.2 \times 10^9 \text{s}^{-1}$, $\eta=0.6$, $\Gamma=0.112$, and $N_{dot}=5 \times 10^{10} \text{cm}^{-2}$. (b) Calculated QD modal gain versus current density curves for values of A as indicated. The curves are computed for $\Delta_{inh}=20 \text{meV}$, $\eta=0.6$, $\Gamma=0.112$, and $N_{dot}=5 \times 10^{10} \text{cm}^{-2}$.

Lorentzian-function fitting, we round off to $\Delta_{inh} = 20\text{meV}$. The computed spontaneous emission spectrum for $\Delta_{inh} = 20\text{meV}$ is plotted in the middle panel of Fig. 3(a). For comparison, we also plotted the calculated spontaneous emission spectra for $\Delta_{inh} = 10\text{meV}$ and $\Delta_{inh} = 30\text{meV}$.

The next step is to match the calculated and measured modal gain versus current density curves. Theoretically, the modal gain is obtained by $G_{modal} = \Gamma G_{material}$, where the mode confinement factor $0.09 \leq \Gamma \leq 0.115$ is estimated from solving Maxwell's equations for laser-field profiles. This confinement factor value is larger than traditional "fill factor" values used for QD lasers because we have defined the QD material gain as distributed over the volume of the embedding QW layer. The material gain used is the peak gain computed for an 8 nm $\text{In}_{0.15}\text{Ga}_{0.85}\text{As}$ QW layer, containing an InAs wetting layer on which sits a density of $N_{dot} = 5 \times 10^{10}\text{cm}^{-2}$ inhomogeneously broadened InAs QDs. For each carrier density, we write a current density

$$J = \frac{1}{\eta} \left[J_{sp} + e(AN + CN^3) \right], \quad (6)$$

where $J_{sp} = 2ed \int_{-\infty}^{\infty} d\omega S(\omega)$ is the spontaneous emission contribution to the current density (factor of 2 is from the 2 TE polarizations in the QW plane and no emission in the TM polarization) and η is an overall efficiency defined as the ratio of the current entering the active region to the total current through the contact, which we hereby assume to be equivalent to the injection efficiency. We assume that the nonradiative carrier loss may be represented by linear and cubic terms with A and C being fitting parameters.

A good fit to experimental data is obtained with $\Delta_{inh} = 20\text{meV}$, $A = 1.2 \times 10^9\text{s}^{-1}$, and $C = 10^{-28}\text{cm}^{-1}\text{s}^{-1}$. The result is plotted as a solid black curve in Figs. 4(a) and 4(b). We do not associate A and C with physical processes because it is well known that physical processes such as defect, radiative, or Auger losses have complicated dependences on total carrier density. Nevertheless, it is interesting to note that the value obtained for A is within the range we reasonably expect for defect related loss in typical QD samples, and the value of C is consistent with an Auger coefficient for a material with band-gap energy around 0.9 eV.¹⁷

Very helpful for confidence in the extracted parameters is the availability of experimental data over a wide range of threshold gain, from below gain saturation, to where the gain is sufficiently saturated to become basically current independent. In the latter case, the gain is largely dependent on the combination of N_{dot} , Γ , and Δ_{inh} , and insensitive to A and η (see Figs. 4(a) and 4(b) for the cases of Δ_{inh} and A, respectively). For each sample, we determine N_{dot} by counting the number of QDs inside a $1\ \mu\text{m} \times 1\ \mu\text{m}$ area, which can be performed sufficiently accurately to pin down Δ_{inh} to better than $\pm 3\text{meV}$. As stated earlier, there is an uncertainty in the confinement factor, resulting in the estimation of $15\text{meV} < \Delta_{inh} < 21\text{meV}$ (see Fig. 5(a)). The curves in Fig. 5 are obtained from calculations where we look for combinations of (Δ_{inh}, Γ) and (A, η) that reproduce the solid curve in either Fig. 4(a) or Fig. 4(b), which best fits the experiment. As to the uncertainty due to non-equilibrium carrier distributions,^{12,18} we address the concern by plotting in Fig. 5(b) the

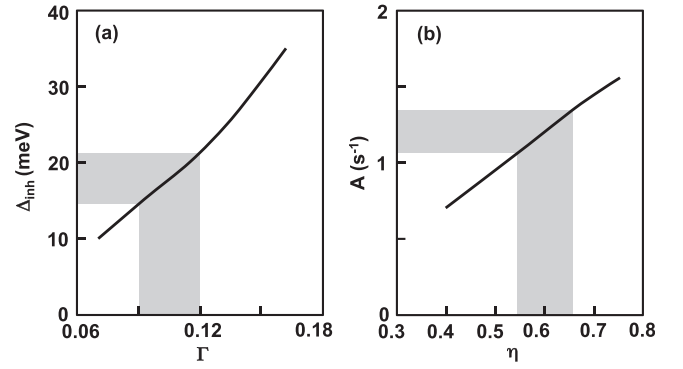


FIG. 5. Combinations of (a) inhomogeneous broadening and confinement factor and (b) linear nonradiative carrier loss coefficient and injection efficiency giving similar modal gain versus current density behavior as solid black curves in Fig. 4, i.e., with combinations ($\Delta_{inh} = 20\text{meV}$, $\Gamma = 0.112$) and ($A = 1.2 \times 10^9\text{s}^{-1}$, $\eta = 0.6$). The shaded regions illustrate sensitivity of Δ_{inh} to Γ and A to η .

dependence of the extracted A on the value of η assumed in the modeling. The variation $10^9\text{s}^{-1} < A < 1.4 \times 10^9\text{s}^{-1}$ from a 10% uncertainty in η still provides us with useful information on sample quality.

We end by noting that a first-principles gain theory has more uses than the extraction of difficult to measure device parameters. With rigorous treatment of relevant physics and minimization of fitting parameters, a model can provide trustworthy assessments of future performance when extrinsic constraints are mitigated. For example, the $\Delta_{inh} = 0$ and 10meV curves in Fig. 4(a) indicate the improvement in gain-current characteristics with better sample uniformity. On the other hand, the $\Delta_{inh} = 30\text{meV}$ curve shows degradation in performance when uniformity is not as good as our present lasers. Interpreting the results differently, the significant difference between the $\Delta_{inh} = 0$ and $\Delta_{inh} > 0$ curves may suggest caution when promoting the advantages of a zero-dimensional system without tempering with the fact that complete elimination of inhomogeneous broadening is impossible.

Equally useful is a comparison of QD versus QW gain performance. A quantitative comparison of InAs QDs with GaInNAs QWs has been previously presented,¹⁹ and here we offer a quantitative experimental comparison with InGaAs QWs. The circles in Fig. 4(a) are from measurements with lasers where gain in each laser is provided by three 8 nm $\text{In}_{0.2}\text{Ga}_{0.8}\text{As}$ QWs. Comparison of QD and QW data shows that for the QD there is potential for lower threshold current (densities), while at the same time indicates stronger gain saturation compared to QWs. The measured QW gain versus current characteristic is reproduced by theory (grey curve), where we use a similar gain model as described by Eqs. (1) and (2). All input parameters are the same except for $\Gamma = 0.054$ and $A = 6.5 \times 10^8\text{s}^{-1}$. No inhomogeneous broadening is introduced in the QW calculations.

To conclude, we propose and analyze a method for extracting inhomogeneous broadening and nonradiative losses in InAs QD lasers by comparing experimental measurements with microscopic theory without the use of free parameters. Such an approach allows for the quantification of the inhomogeneous broadening and nonradiative loss rates, which may be difficult to decouple otherwise since both

result in a degradation of the peak gain. This method may be used to guide material and device design optimizations for QD optoelectronic devices.

This work was supported by Sandia LDRD program, funded by the U.S. Department of Energy under Contract DE-AC04-94AL85000, and by SRC under Contract 2014-EP-2576. We thank Larry Coldren for helpful discussions.

¹P. M. Smowton, P. Blood, and W. W. Chow, *Appl. Phys. Lett.* **76**, 1522 (2000).

²For review see: W. W. Chow and F. Jahnke, *Prog. Quantum Electron.* **37**, 109 (2013).

³M. Asada, Y. Miyamoto, and Y. Suematsu, *IEEE J. Quantum Electron.* **22**, 1915 (1986).

⁴W. W. Chow, P. M. Smowton, P. Blood, A. Girdnt, F. Jahnke, and S. W. Koch, *Appl. Phys. Lett.* **71**, 157 (1997).

⁵T. Inoshita and H. Sakaki, *Phys. Rev. B* **56**, R4355(R) (1997).

⁶J. Seebeck, T. R. Nielsen, P. Gartner, and F. Jahnke, *Phys. Rev. B* **71**, 125327 (2005).

⁷W. E. Lamb, Jr., *Phys. Rev.* **134**, A1429 (1964).

⁸M. Lindberg and S. W. Koch, *Phys. Rev. B* **38**, 3342 (1988).

⁹C. H. Henry, R. A. Logan, and F. R. Merrit, *J. Appl. Phys.* **51**, 3042 (1980).

¹⁰See <http://www.wsi.tum.de/nextnano> for Device Simulator: Nextnano (last accessed November 14, 2007).

¹¹L. A. Coldren, S. W. Corzine, and M. L. Mashanovic, *Diode Lasers and Photonic Integrated Circuits* (Wiley, 2012), pp. 47, 75.

¹²I. P. Marko, A. R. Adams, N. F. Massé, and S. J. Sweeney, *IET Optoelectron.* **8**, 88 (2014).

¹³M. Sugawara, K. Mukai, and H. Shoji, *Appl. Phys. Lett.* **71**, 2791 (1997).

¹⁴H. Shahid, D. T. D. Childs, B. J. Stevens, and R. A. Hogg, *Appl. Phys. Lett.* **99**, 061104 (2011).

¹⁵M. Lorke, W. W. Chow, T. R. Nielsen, J. Seebeck, P. Gartner, and F. Jahnke, *Phys. Rev. B* **74**, 035334 (2006).

¹⁶S. Osborne, P. Blood, P. Smowton, J. Lutti, Y. C. Xin, A. Stintz, D. Huffafer, and L. Lester, *IEEE J. Quantum Electron.* **40**, 1639 (2004).

¹⁷N. F. Massé, A. R. Adams, and S. J. Sweeney, *Appl. Phys. Lett.* **90**, 161113 (2007).

¹⁸P. M. Smowton and P. Blood, *IEEE J. Sel. Top. Quantum Electron.* **3**, 491 (1997).

¹⁹W. W. Chow, M. Lorke, and F. Jahnke, *IEEE J. Sel. Top. Quantum Electron.* **17**, 1349 (2011).